

NUMERICAL EXPLORATION OF THE RANGE OF SHAPE FUNCTIONALS USING NEURAL NETWORKS

ELOI MARTINET AND ILIAS FTOUHI

ABSTRACT. We introduce a novel numerical framework for the exploration of Blaschke–Santaló diagrams, which are efficient tools characterizing the possible inequalities relating some given shape functionals. We introduce a parametrization of convex bodies in arbitrary dimensions using a specific invertible neural network architecture based on gauge functions, allowing an intrinsic conservation of the convexity of the sets during the shape optimization process. To achieve a uniform sampling inside the diagram, and thus a satisfying description of it, we introduce an interacting particle system that minimizes a Riesz energy functional via automatic differentiation in PyTorch. The effectiveness of the method is demonstrated on several diagrams involving both geometric and PDE-type functionals for convex bodies of \mathbb{R}^2 and \mathbb{R}^3 , namely, the volume, the perimeter, the moment of inertia, the torsional rigidity, the Willmore energy, and the first two Neumann eigenvalues of the Laplacian.

1. INTRODUCTION

Visual representations of the range of vector-valued shape functionals—commonly referred to as Blaschke–Santaló diagrams—offer a geometric framework for understanding all possible inequalities that relate prescribed shape functionals within a given class of sets. The terminology honors the pioneering contributions of W. Blaschke [10] and L. Santaló [53], who initiated the systematic study of inequalities linking three geometric functionals on convex bodies. Since then, Blaschke–Santaló diagrams have been widely investigated, particularly in the setting of convex geometry, and also been extended to encompass triplets combining geometric and spectral quantities. For various examples on purely geometric functionals, we refer to the following non-exhaustive list of works [9, 15, 17, 18, 19, 25, 36], and for examples involving both geometric and spectral quantities, we refer to [4, 20, 21, 23, 32, 31, 42, 46]. Also we note that special attention has been given to diagrams involving the Cheeger constant which corresponds to the first eigenvalue of the 1-Laplacian operator with Dirichlet boundary conditions, see [28, 29, 33].

All the aforementioned works focus on establishing theoretical results concerning these diagrams. This includes deriving explicit characterizations in the case of purely geometric functionals, as well as proving qualitative properties when spectral or PDE-related quantities are involved, situations in which obtaining an explicit description is often highly challenging, if not altogether out of reach.

To the best of our knowledge, the numerical investigation of these diagrams has received relatively little attention in the literature. A first natural numerical approach was proposed in [3], where the authors examine the diagram involving the perimeter, the area, and the first Dirichlet eigenvalue by approximating it through point clouds generated from the sampling of thousands of random convex polygons. Subsequently, in [30], I. Ftouhi proposed a hybrid approach that combines theoretical results on the vertical convexity of the diagrams with numerical shape optimization techniques to determine their boundaries. This allowed him to consider diagrams involving the first Dirichlet eigenvalue and geometric quantities such as the perimeter, the area, and the diameter of planar convex sets. Unfortunately, this approach relies on a priori knowledge of the vertical convexity of the diagram, a property that may be highly nontrivial to establish. As a consequence, the method is not readily applicable to more general classes of diagrams. Then came a paper [13] by B. Bogosel, G. Buttazzo and E. Oudet who proposed a method based on Voronoi tessellation and the use of Lloyd’s algorithm to “uniformly”

cover Blaschke–Santaló diagrams. The method was successfully applied to diagrams on matrices involving the trace and determinant functionals as well as to a purely geometric diagram incorporating the moment of inertia, the perimeter, and the area of convex sets with two axes of symmetry. However, as far as we know, it could not be extended to settings involving spectral functionals or more complicated geometries such as general convex sets.

In the present paper, we propose a method based on a new neural network architecture to parametrize convex sets. This parametrization has both the advantages of being smooth and without any constraint. We then show how this new parametrization can be used to uniformly sample Blaschke–Santaló diagrams using a system of interacting particles. Finally, we show how our new method performs on different types of Blaschke–Santaló diagrams.

2. SHAPE REPRESENTATION BY AN INVERTIBLE NEURAL NETWORK

2.1. Previous works. Shape optimization among convex sets has received a lot of attention in the theoretical shape optimization community. Indeed, it is both a natural set of shapes to consider, and at the same time a class that is "rigid" enough so that proving optimality properties is significantly easier than in more generic classes of shapes. On the other hand, numerical shape optimization needs more care to efficiently and precisely take into account the additional convexity constraint.

One of the first approaches was given by E. Oudet in [47], where the convexity constraint is weakly enforced through the introduction of a penalization term measuring the discrepancy between the current set and its convex hull. In subsequent work [41], the same author, together with T. Lachand-Robert suggested representing a convex set as the intersection of half-spaces. By construction, however, this representation precludes the approximation of smooth convex sets. Later, E. Oudet [48] proposed representing a convex set through a discretization of its support function. This approach has since been widely adopted; see, for instance, [2, 7, 12, 14, 30]. At last, we emphasize that these techniques are also implemented using gauge functions, which, like support functions, furnish a parametrization of convex sets.

However, although these latter approaches yield satisfactory results, for instance, in the parametrization of sets of constant width, it presents several technical difficulties that make its implementation somewhat challenging for the purposes considered in the present work. The first difficulty stems from the fact that the support (or gauge) function must satisfy a second-order differential inequality in order to characterize a convex set, thereby leading to a constrained optimization problem. Depending on the chosen parametrization, the convexity inequality can be enforced in an exact (i.e., non-relaxed) form [7, 12], thereby ensuring that the admissible shapes are genuinely convex. However, this has so far only been achieved for two-dimensional convex sets, and, when using a Fourier basis discretization, it leads to non-linear constraints on the coefficients. In [2], the method based on the truncation of the Fourier expansion is generalized to the three-dimensional setting. However, the semi-definite constraint is relaxed to a linear one, which can result in a loss of convexity of the admissible shapes, sometimes to a considerable extent.

In contrast to previous methods, the approach in [6] utilizes a direct triangulation-based shape variation framework, wherein the deformation field is constrained to satisfy a convexity-preserving criterion.

Finally, several neural-network-based representations of convex sets have already been proposed, either by enforcing the convexity of the learned level-set function [45] or by adopting a phase-field formulation [26].

2.2. Proposed approach. The objective of this section is to propose a completely unconstrained method that allows one to easily represent convex sets in arbitrary dimension, and for which the usual shape functions can be easily computed, including the ones involving curvature or PDE-related terms. Moreover, since we will perform extensive multi-shape optimization, we want this parametrization to integrate automatic differentiation for easy optimization. Hence, we have chosen to represent convex sets as the image of specific diffeomorphisms of the unit ball, where the diffeomorphism is given by a new neural network architecture. Note that the idea of representing a shape as a neural

diffeomorphism has already been considered in [8], where authors utilize symplectic maps to represent geometry, thereby ensuring intrinsic measure conservation.

In what follows, \mathcal{K}_d will denote the class of convex bodies of \mathbb{R}^d that contain the origin in their interior. As the shape functionals considered hereafter are translation-invariant, this assumption entails no loss of generality.

Let $p : \mathbb{R}^d \rightarrow \mathbb{R}$ be a positive, continuous, and sublinear function, i.e., $p(\lambda x) = \lambda p(x)$ and $p(x+y) \leq p(x) + p(y)$, for every $\lambda > 0$ and $x, y \in \mathbb{R}^d$. Then, the set

$$\{x \in \mathbb{R}^d : p(x) < 1\}$$

is an open and convex domain. Conversely, every open and convex body of \mathbb{R}^d is, up to a translation, of the form above for a certain continuous, positive, and sublinear function which corresponds to its gauge function. Using these properties, we can show that convex sets can be described as homeomorphisms of the ball.

Proposition 2.1. *Let p be a positive, continuous, and sublinear function. The function $\phi : x \mapsto \frac{\|x\|}{p(x)}x$ is a homeomorphism from B to $\phi(B)$ and the image set $\phi(B)$ is convex.*

Proof. Let $K := \{y \in \mathbb{R}^d : p(y) < 1\}$. For $x \in B$, we have

$$p(\phi(x)) = \frac{\|x\|}{p(x)}p(x) = \|x\| < 1.$$

Hence, $\phi(B) \subset K$. On the other hand, if $y \in K$, then $x := \frac{p(y)}{\|y\|}y \in B$ and $y = \phi(x)$. Therefore, $\phi(B) = K$ is convex and ϕ is a homeomorphism. \square

In what follows, convex sets will be represented via such homeomorphisms. Now, it is important to be able to faithfully represent any positive, continuous, and sublinear function p . To this end, we will derive an architecture of a neural network $p_\theta : \mathbb{R}^d \rightarrow \mathbb{R}$ (where θ represents the parameters) which intrinsically satisfies those constraints. A reasonable choice of architecture would be

$$p_\theta(x) = \max_{1 \leq i \leq N} (w_i \cdot x),$$

with $w_i \in \mathbb{R}^d$ for all i (i.e., a single layer neural network with MaxOut activation function [38]). This is motivated by the fact that any sublinear function is a supremum of linear forms. Then we can set $\phi_\theta(x) := \frac{\|x\|}{p_\theta(x)}x$ to get that $\phi_\theta(B)$ is convex. However, it may be more convenient to be able to define a neural network that is smooth (at least at the boundary of B) in order to compute usual quantities of interest (normals, curvature, etc). A natural idea, used, for example, in [26], is to replace the previous representation $p_\theta(x) = \max_{1 \leq i \leq N} (w_i \cdot x)$ by a smoothed version obtained via the LogSumExp (LSE) function:

$$(1) \quad p_\theta(x) = \beta \text{LSE}(W^T x),$$

where $\beta > 0$, $W = (w_1 \cdots w_N) \in \mathbb{R}^{d \times N}$, and

$$\text{LSE}(y) := \log \sum_{i=1}^N e^{y_i}.$$

Note that although β is not strictly required, it is directly related to the scale of the shape being represented, making scale adjustments more manageable for the optimizer.

It is well known that $\alpha^{-1} \text{LSE}(\alpha y)$ converges to $\max_{1 \leq i \leq N} y_i$ as $\alpha \rightarrow \infty$. The function p_θ can be seen as a single-layer neural network with learnable parameters $\theta = \{\beta, W\}$.

Note that in eq. (1), the function p_θ is no longer sublinear. However, we can define a function which agrees with the log-sum-exp on the sphere and is sublinear as one sees in the following proposition.

Proposition 2.2. *The function*

$$(2) \quad p_\theta(x) := \beta \|x\| \text{LSE} \left(W^T \frac{x}{\|x\|} \right)$$

is continuous, sublinear, and is C^∞ on $\mathbb{R}^n \setminus \{0\}$.

The proof of this proposition (and the following one) will be provided in an upcoming paper interested in the representation of shapes using invertible neural networks [44].

The set $\Omega_\theta := \phi_\theta(B)$ is convex by the construction of the neural network $\phi_\theta(x) := \frac{\|x\|}{p_\theta(x)} x$. However, it is of core interest to know whether every convex set can be represented using a neural network. Since any K_θ must be smooth, this would not be the case; however, in the forthcoming work [44], E. Martinet proves the following “Universal Approximation Theorem”, which ensures that this approach yields a consistent approximation of convex sets.

Theorem 2.3. *Define*

$$\mathcal{K}_d^{NN} := \left\{ \Omega_\theta : \beta > 0, W \in \mathbb{R}^{d \times N}, N \in \mathbb{N} \right\}$$

as the set of convex bodies that can be represented by the architecture given by eq. (2). Then \mathcal{K}_d^{NN} is dense in \mathcal{K}_d with respect to the Hausdorff distance.

2.3. Encoding symmetries. Oftentimes, one may be interested in convex bodies that satisfy certain symmetries. Let G be a finite subgroup of isometries of \mathbb{R}^n and $\rho_\theta : \mathbb{R}^n \rightarrow \mathbb{R}$ be some neural network given in the previous section, and define

$$(3) \quad \phi_\theta^G(x) := x \frac{\|x\|}{\sum_{g \in G} \rho_\theta(g^{-1}x)}.$$

Then, ϕ_θ^G is G -equivariant, which means that $g.\phi_\theta^G(x) = \phi_\theta^G(g.x)$. This, in turn, implies that the set $\Omega_\theta := \phi_\theta^G(B)$ is G -invariant, meaning that $g.\Omega_\theta = \Omega_\theta$ for all $g \in G$.

3. SAMPLING THE DIAGRAM

Let us denote by $\mathcal{D} := \{F(\Omega) : \Omega \in \mathcal{K}_d\}$ the Blaschke–Santaló diagram of interest, where $F : \mathcal{K}_d \rightarrow \mathbb{R}^n$ is some vector-valued shape functional. In order to uniformly sample the diagram \mathcal{D} , we will look for a distribution of repulsive electric charges that are at equilibrium inside the diagram \mathcal{D} . Formally speaking, this amounts to minimizing the so-called *Riesz energy*:

$$(4) \quad \min_{y_1, \dots, y_N \in \mathcal{D}} \sum_{1 \leq i \neq j \leq N} |y_i - y_j|^{-s} \iff \min_{\Omega_1, \dots, \Omega_N \in \mathcal{K}_d} \sum_{1 \leq i \neq j \leq N} |F(\Omega_i) - F(\Omega_j)|^{-s},$$

with $s > 0$. Note that when $s \rightarrow \infty$, eq. (4) reduces to the famous *sphere-packing problem*

$$\min_{y_1, \dots, y_N \in \mathcal{D}} \max_{1 \leq i \neq j \leq N} |y_i - y_j|.$$

With that in mind, it is reasonable to expect that for s large enough, the points will distribute uniformly in \mathcal{D} , which turns out to be indeed the case, as shown by *Poppy-seed Bagel Theorem* [16]. For simplification purposes, we state the theorem in the context of smooth manifolds:

Theorem 3.1 (Th. 8.5.2 in [16]). *Let $A \subset \mathbb{R}^p$ be a smooth, compact submanifold of dimension $d < s$. Let $\omega_N = (y_1, \dots, y_N) \in A^N$ be a minimizing configuration of*

$$\min_{(y_1, \dots, y_N) \in A^N} \sum_{1 \leq i \neq j \leq N} |y_i - y_j|^{-s}.$$

Then, the measure $\nu(\omega_N) := \frac{1}{N} \sum_{y \in \omega_N} \delta_y$ weakly converges to the uniform probability measure on A .

In the following, we formulate a refined version of the theorem, ensuring that the minimal pairwise distance between points is bounded below by a positive constant.

Theorem 3.2 (Th. 8.8.1 in [16]). *Under the assumptions of the previous theorem and the fact that A is path-connected, there exists a constant $C > 0$ such that for all $N \geq 2$,*

$$\min_{\substack{x,y \in \omega_N \\ x \neq y}} |x - y| \geq \frac{C}{N^{1/d}}.$$

Using those theorems as motivation for our method (although, we do not necessarily satisfy the assumptions), we will numerically approximate eq. (4) by

$$(5) \quad \min_{\theta_1, \dots, \theta_N} \sum_{1 \leq i \neq j \leq N} |F(\Omega_{\theta_i}) - F(\Omega_{\theta_j})|^{-s}.$$

Using PyTorch [49], this problem can be easily solved by some l-BFGS method, as long as the derivative of the function $\theta \mapsto F(\Omega_\theta)$ can be automatically computed. We shall assume this condition to hold throughout the remainder of the paper.

4. NUMERICAL COMPUTATION OF THE INVOLVED SHAPE FUNCTIONALS

In this section, we describe in detail the computation of several common shape functionals, highlighting the advantages offered by PyTorch's automatic differentiation capabilities.

4.1. Integral quantities. For integral quantities, the idea is simply to formulate the computations on the reference domain. To this purpose, we use the volumic and surfacic changes of variable formulas

$$\int_{\Omega_\theta} f dx = \int_B (f \circ \phi_\theta) \text{Jac}(\phi_\theta) dx \quad \text{and} \quad \int_{\partial\Omega_\theta} g d\sigma = \int_{\partial B} (g \circ \phi_\theta) \text{Jac}_{\partial B}(\phi_\theta) d\sigma,$$

where

$$\text{Jac}(\phi_\theta) = |\det(D\phi_\theta)| \quad \text{and} \quad \text{Jac}_{\partial B}(\phi_\theta) = \text{Jac}(\phi_\theta) |(D\phi_\theta)^{-T} n_B|,$$

and $n_B(x) := x$ on ∂B is the unit outward normal vector. We will apply those formulas to compute the volume Vol, perimeter Per and moment of inertia W of a shape Ω_θ .

Remark 4.1. *Note that nowhere we actually need the convexity or special form of ϕ_θ . This approach can and will be extended to an arbitrary invertible neural network ϕ_θ is a forthcoming paper.*

For the volume, we can simply compute

$$\text{Vol}(\Omega_\theta) = \int_B \text{Jac} \phi_\theta dx.$$

We proceed similarly for the moment of inertia, defined as

$$W(\Omega_\theta) := \int_{\Omega} |x - x_{\Omega_\theta}|^2 dx,$$

where $x_{\Omega_\theta} := \int_{\Omega_\theta} x dx$ is the center of mass of Ω_θ . By a change of variables, the latter can be expressed as

$$x_{\Omega_\theta} = \int_B \phi_\theta(x) \text{Jac} \phi_\theta(x) dx,$$

while the former is

$$W(\Omega_\theta) = \int_B |\phi_\theta(x) - x_{\Omega_\theta}|^2 \text{Jac} \phi_\theta(x) dx.$$

In the same fashion, the perimeter can be pulled back to the boundary of the reference domain and is computed as follows

$$\text{Per}(\Omega_\theta) = \int_{\partial B} \text{Jac}_{\partial B}(\phi_\theta) d\sigma.$$

4.2. Curvature-related quantities. The mean curvature of a smooth set Ω at $y \in \partial\Omega$ can be defined as

$$H_\Omega(y) := \frac{1}{d-1} \operatorname{div} n_\Omega(y) = \frac{1}{d-1} \operatorname{Tr}(Dn_\Omega(y)),$$

where n_Ω is a unit length extension of the normal vector to \mathbb{R}^d , see for example [39, Proposition 5.4.8]. This quantity appears in the *Willmore energy*:

$$E(\Omega) := \int_{\partial\Omega} H_\Omega^2(y) dy.$$

In the case of a parameterized set Ω_θ , the normal vector n_{Ω_θ} can be expressed for $x \in \partial B$ as

$$n_{\Omega_\theta}(\phi_\theta(x)) = \frac{(D\phi_\theta)^{-T}(x)n_B(x)}{\left|(D\phi_\theta)^{-T}(x)n_B(x)\right|},$$

and the change of variable formula leads to

$$\int_{\partial\Omega_\theta} H_{\Omega_\theta}^2(y) dy = \int_{\partial B} H_{\Omega_\theta}^2(\phi_\theta(x)) \operatorname{Jac}_{\partial B}(\phi_\theta(x)) dx.$$

4.3. PDE-related quantities. In the sequel, we will consider several PDE related quantities, namely the torsion and Laplace eigenvalues of a domain. The torsion of a domain Ω is defined as

$$T(\Omega) = \int_{\Omega} u dx,$$

where $u \in H_0^1(\Omega)$ is the solution to

$$(6) \quad \begin{cases} -\Delta u &= 1 & \text{in } \Omega, \\ u &= 0 & \text{on } \partial\Omega. \end{cases}$$

Equivalently, by taking $\phi(x) = u(x) + \frac{x_1^2}{2}$, we can look for a function ϕ which is solution to

$$(7) \quad \begin{cases} -\Delta\phi &= 0 & \text{in } \Omega, \\ \phi &= \frac{x_1^2}{2} & \text{on } \partial\Omega. \end{cases}$$

One may then seek a solution ϕ expressed as a linear combination of fundamental solutions, namely,

$$\phi(x) := \sum_{i=1}^n c_i \psi(x - y_i),$$

where ψ is the fundamental solution to $-\Delta\psi = \delta_0$ in $\mathbb{R}^d - \{0\}$ and $y_1, \dots, y_n \in \Omega^c$. Since ϕ is a harmonic function in Ω , we only have to fit the boundary condition, for instance, in an L^2 sense, which amounts to solving

$$\min_{c_1, \dots, c_n \in \mathbb{R}} \int_{\partial\Omega} \left| \phi(x) - \frac{x_1^2}{2} \right|^2 d\sigma.$$

Since this integral cannot be analytically computed for a general Ω , it is discretized and the resulting least squares problem is solved. This method takes inspiration from [40], and in the Method of Fundamental Solutions that have already been used to solve shape optimization problems [2, 11].

A key advantage of the present method is that it allows to autodifferentiate the resulting $\theta \mapsto T(\Omega_\theta)$ with respect to the parameters of the network, since every operation is supported by PyTorch (in particular, the solution of the least square problem via `torch.linalg.lstsq`).

As previously mentioned, we will also consider the computation of Laplace eigenvalues with a homogeneous Neumann boundary condition i.e., positive values for which the equation

$$\begin{cases} -\Delta u &= \mu u & \text{in } \Omega, \\ \partial_n u &= 0 & \text{on } \partial\Omega, \end{cases}$$

admits non-trivial solutions.

It is well known that for a Lipschitz domain Ω , the spectral theorem guarantees that there exists an increasing sequence of eigenvalues

$$0 = \mu_0(\Omega) \leq \mu_1(\Omega) \leq \cdots \leq \mu_k(\Omega) \leq \cdots \rightarrow \infty.$$

In order to numerically approximate the eigenvalues, we will use a mesh free RBF-Galerkin method as described in [57]. Let us quickly explain how this works in our case. Let

$$\int_{\Omega_\theta} \nabla u \cdot \nabla u dx = \mu \int_{\Omega_\theta} u u dx,$$

$u, v \in H^1(\Omega)$ be the weak formulation of eq. (10). Using change of variables, we can pull back the equation over the reference domain B , which reads

$$\int_B A_\theta \nabla u \cdot \nabla v dx = \mu \int_B (\text{Jac}\phi_\theta) u v dx,$$

for all $u, v \in H^1(B)$, where $A_\theta := (\text{Jac}\phi_\theta)(D\phi_\theta)^{-1}(D\phi_\theta)^{-T}$. This problem is then discretized on a subspace spanned by radial basis functions (RBFs) $\varphi_i(x) := \psi(|x - x_i|)$, $x_i \in \Omega$, leading to a system

$$K_\theta \bar{u} = \mu M_\theta \bar{u},$$

where

$$[K_\theta]_{ij} = \int_B A_\theta \nabla \varphi_i \cdot \nabla \varphi_j dx \quad \text{and} \quad [M_\theta]_{ij} = \int_B (\text{Jac}\phi_\theta) \varphi_i \varphi_j dx.$$

Since PyTorch does not currently offer automatic differentiation for generalized eigenvalue problems, we instead solve the equivalent problem

$$(8) \quad L_\theta^{-1} K_\theta L_\theta^{-T} \bar{u} = \mu \bar{u},$$

where L_θ is obtained via the Cholesky decomposition $M_\theta = L_\theta L_\theta^T$.

This method is chosen because it provides theoretical convergence guarantees (unlike other meshless methods relying on the strong formulation of the PDE like, for instance, the Kansa method [27], or PINN-based methods) and is easy to implement in PyTorch. An alternative, robust approach would consist in using finite element methods. Such a strategy would, however, require additional care to ensure a consistent interaction between the finite element solver and PyTorch, particularly with regard to the integration of automatic differentiation.

4.4. A note on the practical computation of shape quantities. In practice, all Jacobians can be computed using automatic differentiation. In this regard, our method is highly flexible, and can be readily adapted to a wide range of problems.

To compute integral quantities, one needs to choose some discretization of B and ∂B . One might choose to use some Monte-Carlo approach, which has the advantage of being insensible to the curse of dimensionality. However, we will only consider convex sets in \mathbb{R}^2 and \mathbb{R}^3 , and we will use an l-BFGS algorithm with line-search, which is very sensitive to noise. Hence, we decided to discretize B by lattice points, while the sphere ∂B is sampled via a Fibonacci lattice [37].

If the convex sets become too flat during the optimization, the computation of geometric and spectral quantities often loses accuracy. In order to avoid this, we add a regularizer based on the Jacobian of ϕ_θ . More precisely, we add a regularizer based on the maximal condition number of the Jacobian over B . The condition number of a matrix $A \in \mathbb{R}^{d \times d}$, denoted $\text{cond}A$, is the ratio between its largest and smallest singular value. The regularizer then reads

$$\sum_{i=1}^N \|\text{cond}\text{Jac}\phi_{\theta_i}\|_\infty.$$

Hence, the total loss function that we minimize is

$$L(\theta_1, \dots, \theta_N) = \sum_{1 \leq i \neq j \leq N} |F(\Omega_{\theta_i}) - F(\Omega_{\theta_j})|^{-s} + \alpha \sum_{i=1}^N \|\text{cond}\text{Jac}\phi_{\theta_i}\|_\infty.$$

4.5. Code availability. All these functions have been fully implemented in PyTorch and integrated into an easy-to-use package, available at <https://github.com/EloiMartinet/ConvexShapeOpt>. Detailed installation instructions and comprehensive documentation are provided to assist the reader in conducting their own numerical experiments.

To facilitate reproducibility and ease of use, a collection of notebooks is available here, allowing the reader to experiment with the code without any prior installation. The repository contains three scripts that install the package and solve representative shape optimization problems.

5. OBTAINED RESULTS

5.1. The diagram \mathbf{Vol} , \mathbf{Per} , \mathbf{W} . In this section, we are interested in the diagram of the volume, the perimeter and the moment of inertia, see Section 4.1 for the definitions. Our method is applied to obtain numerical descriptions for three classes of sets: the planar convex domains, the planar convex domains with two orthogonal axes of symmetries a class that has been studied in detail in [36], and the convex domains in three dimensions.

A first step is to reduce the three quantities into two scale invariant ones. Using a change of variables, we can easily show that

$$\mathbf{Vol}(t\Omega) = t^d \mathbf{Vol}(\Omega), \quad \mathbf{Per}(t\Omega) = t^{d-1} \mathbf{Per}(\Omega), \quad \text{and} \quad \mathbf{W}(t\Omega) = t^{d+2} \mathbf{W}(\Omega),$$

which means that the quantities

$$\frac{\mathbf{Vol}(\Omega)^{(d+2)/d}}{\mathbf{W}(\Omega)} \quad \text{and} \quad \frac{\mathbf{Vol}(\Omega)}{\mathbf{Per}(\Omega)^{d/(d-1)}}$$

are scale-invariant. Moreover, the isoperimetric inequality implies that

$$\frac{\mathbf{Vol}(\Omega)}{\mathbf{Per}(\Omega)^{d/(d-1)}} \leq \frac{\mathbf{Vol}(B)}{\mathbf{Per}(B)^{d/(d-1)}}.$$

One can apply the Hardy-Littlewood inequality for symmetric rearrangements to show that

$$\frac{\mathbf{Vol}(\Omega)^{(d+2)/d}}{\mathbf{W}(\Omega)} \leq \frac{\mathbf{Vol}(B)^{(d+2)/d}}{\mathbf{W}(B)},$$

where B is any ball (see [52, Chapter 7, Section 2]). Hence, by taking

$$x(\Omega) = \frac{\mathbf{Vol}(\Omega)^{(d+2)/d}}{\mathbf{W}(\Omega)} \frac{\mathbf{W}(B)}{\mathbf{Vol}(B)^{(d+2)/d}} \quad \text{and} \quad y(\Omega) = \frac{\mathbf{Vol}(\Omega)}{\mathbf{Per}(\Omega)^{d/(d-1)}} \frac{\mathbf{Per}(B)^{d/(d-1)}}{\mathbf{Vol}(B)},$$

we have that the diagram

$$\mathcal{D}_{VPW}^d := \{(x(\Omega), y(\Omega)) : \Omega \in \mathcal{K}_d\}$$

is a subset of the unit square $[0, 1]^2$.

Remark 5.1. *Rescaling the problems so that the diagram fits within $[0, 1]^2$ requires additional information about the shape functions involved, but this is by no means required by the method itself. Nevertheless, for the sake of consistency, we will adopt this rescaling throughout what follows.*

5.1.1. The diagram \mathbf{Vol} , \mathbf{Per} , \mathbf{W} for planar convex bodies. When considering planar convex sets $d = 2$, we take

$$x(\Omega) = \frac{1}{2\pi} \frac{\mathbf{Vol}(\Omega)^2}{\mathbf{W}(\Omega)} \quad \text{and} \quad y(\Omega) = 4\pi \frac{\mathbf{Vol}(\Omega)}{\mathbf{Per}(\Omega)^2},$$

In this case, we recall the classic inequality obtained by G. Pólya in [51, Theorem 1]

$$\frac{\mathbf{Vol}(\Omega)\mathbf{Per}(\Omega)^2}{\mathbf{W}(\Omega)} > 48,$$

which is sharp as the equality asymptotically holds when considering a sequence of thinning stadiums. This inequality is then written in terms of $x(\Omega)$ and $y(\Omega)$ as follows

$$y(\Omega) < \frac{\pi^2}{6} x(\Omega).$$

Also, we recall the classic conjecture by G. Pólya that states that for all planar convex sets

$$\frac{\text{Vol}(\Omega)\text{Per}(\Omega)^2}{W(\Omega)} \leq 108,$$

with equality if and only if Ω is an equilateral triangle. This estimate is written in terms of $x(\Omega)$ and $y(\Omega)$ as follows:

$$y(\Omega) \geq \frac{2\pi^2}{27} x(\Omega).$$

Note that this diagram has been studied recently in [36] in the planar case $d = 2$ for convex bodies with two orthogonal axes of symmetry, which is addressed in Section 5.1.2.

We now solve eq. (5) for $F(\Omega) := (x(\Omega), y(\Omega))$ where $\Omega \subset \mathcal{K}_d$, with $d \in \{2, 3\}$. Note that while the \mathbb{R}^2 case can still run on a laptop, the \mathbb{R}^3 case runs in a few hours on an Nvidia h100 GPU. This is due to the fact that the number of quadrature points necessary to compute the quantities of interest to the desired accuracy in \mathbb{R}^3 is significantly larger than in \mathbb{R}^2 , preventing the computational graph of PyTorch to fit in a standard laptop RAM.

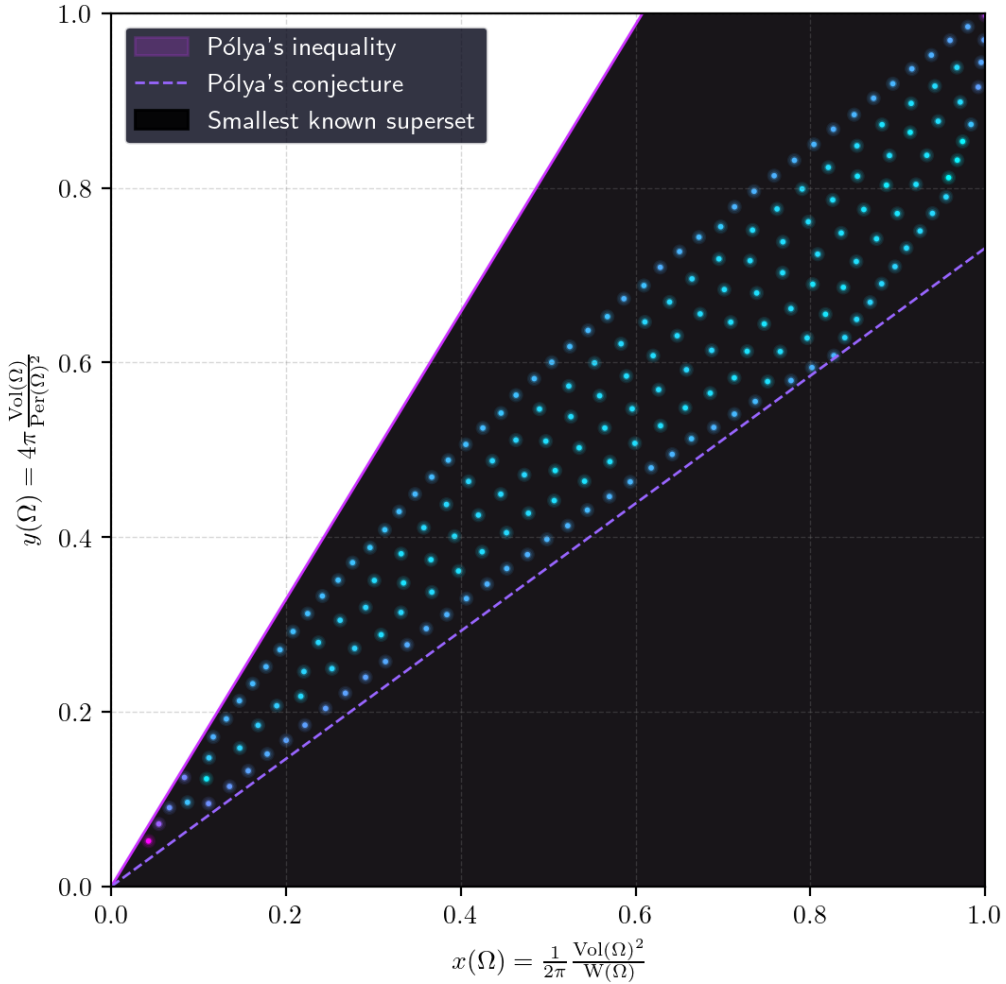


FIGURE 1. Numerical approximation of the diagram \mathcal{D}_{VPW}^2 for $d = 2$.

The resulting diagram is displayed in fig. 1. The black region represents the smallest known set that contains the diagram. The blue points are the optimal points given by our method. As you can see, the points are uniformly distributed in the diagram.

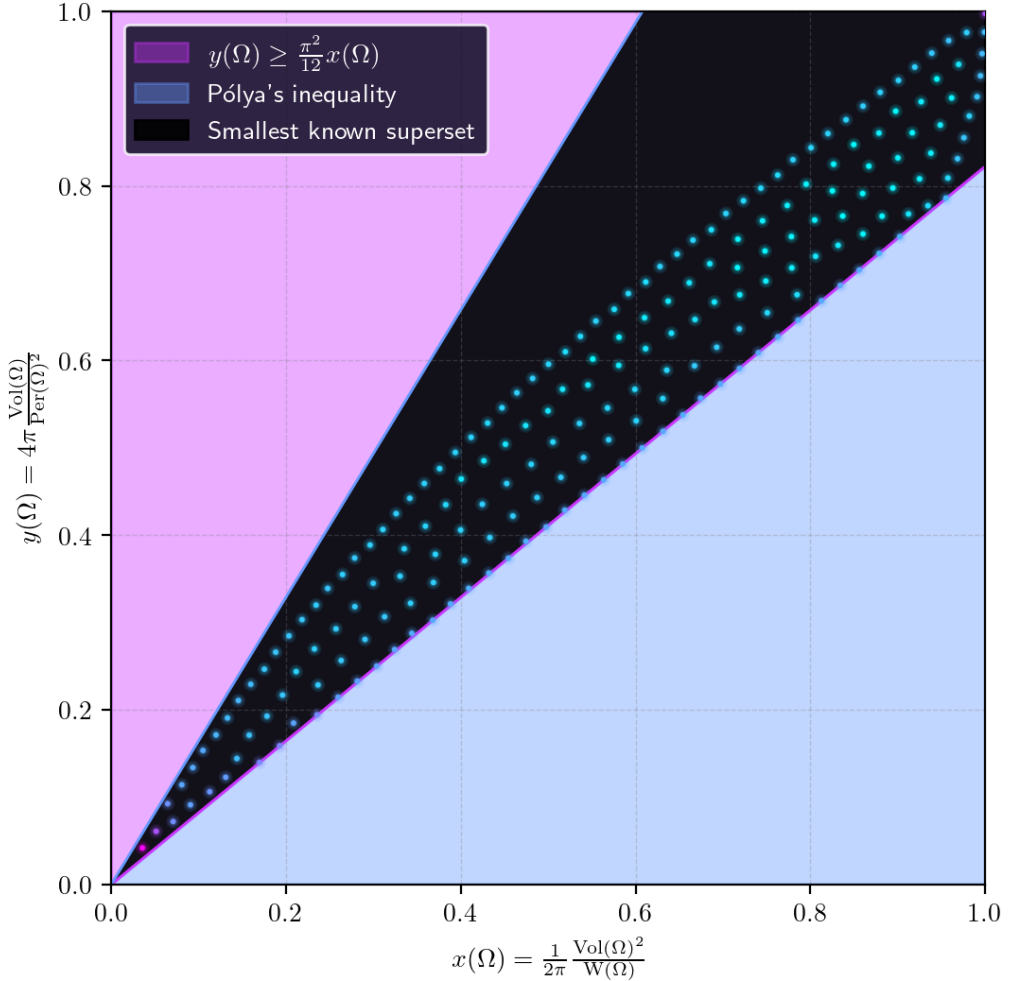


FIGURE 2. Numerical approximation of the diagram \mathcal{D}_{VPW}^2 for planar and doubly symmetric convex bodies, along with the theoretically known lower boundary.

A visualization of the sets comprising the diagram can be found here. As observed, the neural network representation of the convex shapes allows for both smooth and polygonal shapes. The upper part of the boundary seems to be realized by smooth domains resembling stadiums, while the leftmost lower part is apparently realized by isosceles triangles. We see that no points are sampled near the origin. The reason is the Jacobian regularizer preventing flattening sets. Indeed, a small y indicates a large isoperimetric ratio, which can only be attained for very flat convex sets.

5.1.2. *The diagram Vol, Per, W for doubly symmetric planar convex bodies.* We check that our method correctly samples the diagram studied in [36], where planar convex bodies with two orthogonal axes of symmetry are considered. In the cited paper, a large part of the lower boundary is explicitly described (see [36, Corollary 5.2]) by the inequality

$$y(\Omega) \geq \frac{\pi^2}{12} x(\Omega).$$

By taking the subgroup of isometries of \mathbb{R}^2

$$G := \{(x, y) \mapsto (x, y), \quad (x, y) \mapsto (-x, y), \quad (x, y) \mapsto (x, -y), \quad (x, y) \mapsto (-x, -y)\}$$

in eq. (3), we are able to represent only convex sets with horizontal and vertical reflection symmetries. The resulting diagram is displayed in fig. 2.

A visualization of the sets comprising the diagram can be found here. We observe that our method accurately recovers the known part of lower boundary of the diagram, which is attained by rhombi, see [36, Theorem 5.1]. On the other hand, the (symmetric) sets located on the upper boundary seem to be the same as the ones obtained for the general case presented in fig. 1.

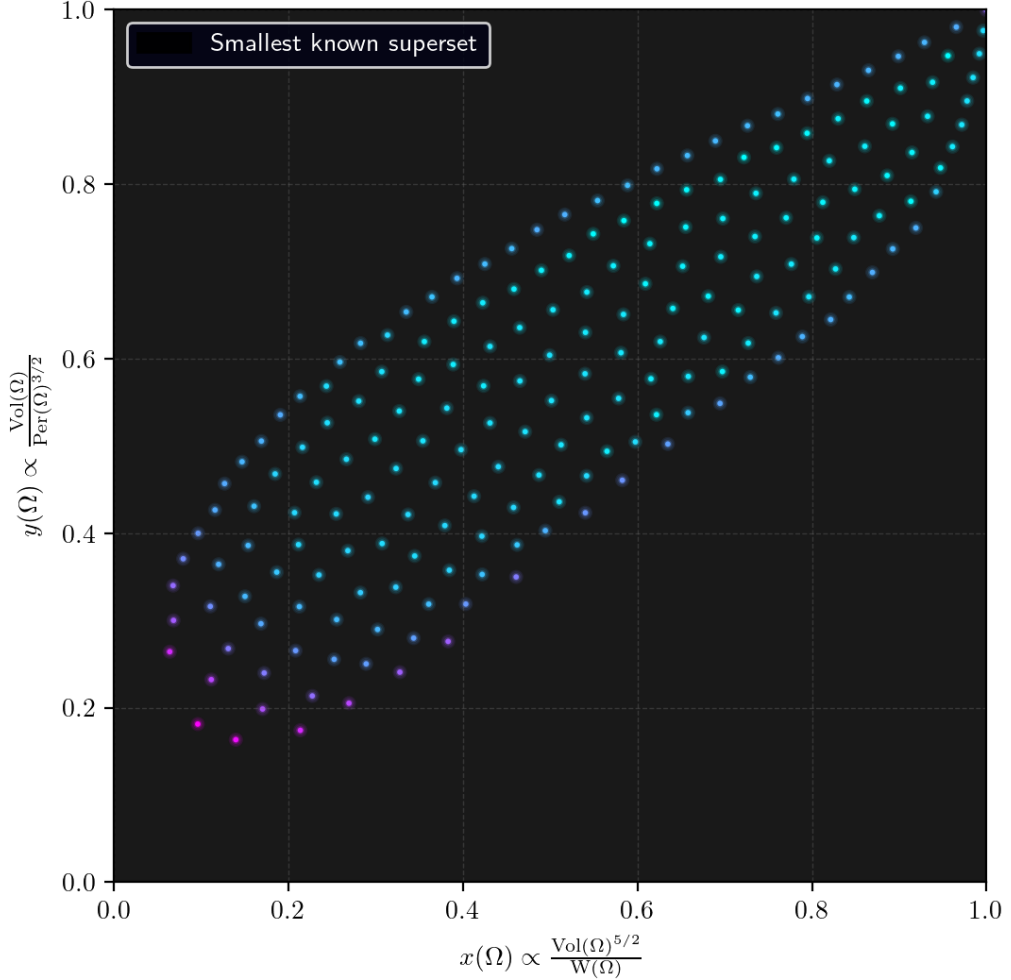


FIGURE 3. Numerical approximation of the diagram \mathcal{D}_{VPW}^3 for $d = 3$

5.1.3. *The diagram Vol, Per, W for convex bodies in three dimensions.* We show that the method also allow for diagrams involving 3 dimensional convex sets. In this case,

$$x(\Omega) = \left(\frac{3}{4}\right)^{5/3} \left(\frac{4}{5\pi^{2/3}}\right) \frac{\text{Vol}(\Omega)^{5/3}}{\text{W}(\Omega)} \quad \text{and} \quad y(\Omega) = 6\sqrt{\pi} \frac{\text{Vol}(\Omega)}{\text{Per}(\Omega)^{3/2}}.$$

The resulting diagram is displayed in fig. 3. A visualization of the sets comprising the diagram can be found here. The upper part of the boundary appears to be attained by sausage-shaped domains, namely domains obtained as revolutions of stadiums about their axes of symmetry. The leftmost lower portion is apparently attained by flattening polyhedra.

5.2. **The diagram Vol, Per, T.** To illustrate the applicability of our method to more complex PDE-dependent problems, we consider a diagram involving the torsional rigidity functional. Let us recall that the torsional rigidity of a domain Ω is given by

$$T(\Omega) = \int_{\Omega} u dx,$$

where $u \in H_0^1(\Omega)$ is the solution of

$$(9) \quad \begin{cases} -\Delta u &= 1 \text{ in } \Omega, \\ u &= 0 \text{ on } \partial\Omega. \end{cases}$$

A straightforward change of variables shows that $T(t\Omega) = t^{d+2}T(\Omega)$. In order to obtain scale-invariant quantities and to have a diagram contained in the unit square $[0, 1]^2$, we set

$$x(\Omega) := \frac{\text{Vol}(\Omega)^{(d-1)/d}}{\text{Per}(\Omega)} \cdot \frac{\text{Per}(B)}{\text{Vol}(B)^{(d-1)/2}} \quad \text{and} \quad y(\Omega) = \frac{\text{Vol}(B)^{(d+2)/d}}{T(B)} \cdot \frac{T(\Omega)}{\text{Vol}(\Omega)^{(d+2)/d}},$$

then, consider the diagram $\mathcal{D}_{VPT} := \{(x(\Omega), y(\Omega)) : \Omega \in \mathcal{K}_d\}$. The fact that $y(\Omega) \in [0, 1]$ is a consequence of the classic Saint-Venant inequality [24].

Note that, by separation of variables, the torsion of the unit ball B can be computed explicitly and is then given by $T(B) = \omega_d/(d(d+2))$, where ω_d is the Lebesgue measure of B .

When $d = 2$, Makai [43] also proved the following inequality:

$$\frac{T(\Omega)\text{Per}(\Omega)^2}{\text{Vol}(\Omega)} \leq \frac{2}{3},$$

while Pólya [50] showed that

$$\frac{T(\Omega)\text{Per}(\Omega)^2}{\text{Vol}(\Omega)} \geq \frac{1}{3}.$$

In terms of x and y , those inequalities translate to

$$\frac{2}{3}x(\Omega)^2 \leq y(\Omega) \leq \frac{4}{3}x(\Omega)^2,$$

which yields the inclusion

$$\mathcal{D}_{VPT}^2 \subset \left\{ (x, y) : \frac{2}{3}x^2 \leq y \leq \frac{4}{3}x^2 \right\}.$$

The resulting diagram is displayed in fig. 4. A visualization of the sets comprising the diagram can be found [here](#).

5.3. The diagram Vol , μ_1 , μ_2 . In this section, we study the diagram of the volume and the first two non-trivial Neumann eigenvalues, which are positive μ for which the problem

$$(10) \quad \begin{cases} -\Delta u &= \mu u \text{ in } \Omega, \\ \partial_n u &= 0 \text{ on } \partial\Omega, \end{cases}$$

admits non-trivial solutions. We note that this diagram has been studied by P. Antunes and A. Henrot in [4].

It can be shown that for every $k \in \mathbb{N}$, the function $t \mapsto \mu_k(t\Omega)$ is (-2) -homogeneous, which implies that the quantity

$$\text{Vol}(\Omega)^{2/d} \mu_k(\Omega)$$

is scale-invariant for every $k \in \mathbb{N}$. Using Brouwer's fixed point argument and properties of the eigenfunctions of the ball, Weinberger showed that for $k = 1$ and every $d \in \mathbb{N}^*$, the previous quantity is maximized by the ball [56]. Using a more involved argument of topological degree theory, D. Bucur and A. Henrot [22] demonstrated that the previous quantity is maximized by the union of two disjoint balls of the same measure, for $k = 2$ and all $d \in \mathbb{N}^*$.

For $d = 2$, we consider the quantities

$$x(\Omega) := \frac{\text{Vol}(\Omega)\mu_1(\Omega)}{\text{Vol}(B)\mu_1(B)} \quad \text{and} \quad y(\Omega) := \frac{\text{Vol}(\Omega)\mu_2(\Omega)}{\text{Vol}(B \sqcup B)\mu_2(B \sqcup B)},$$

where $B \sqcup B$ here denotes the union of two disjoint balls of the same measure.

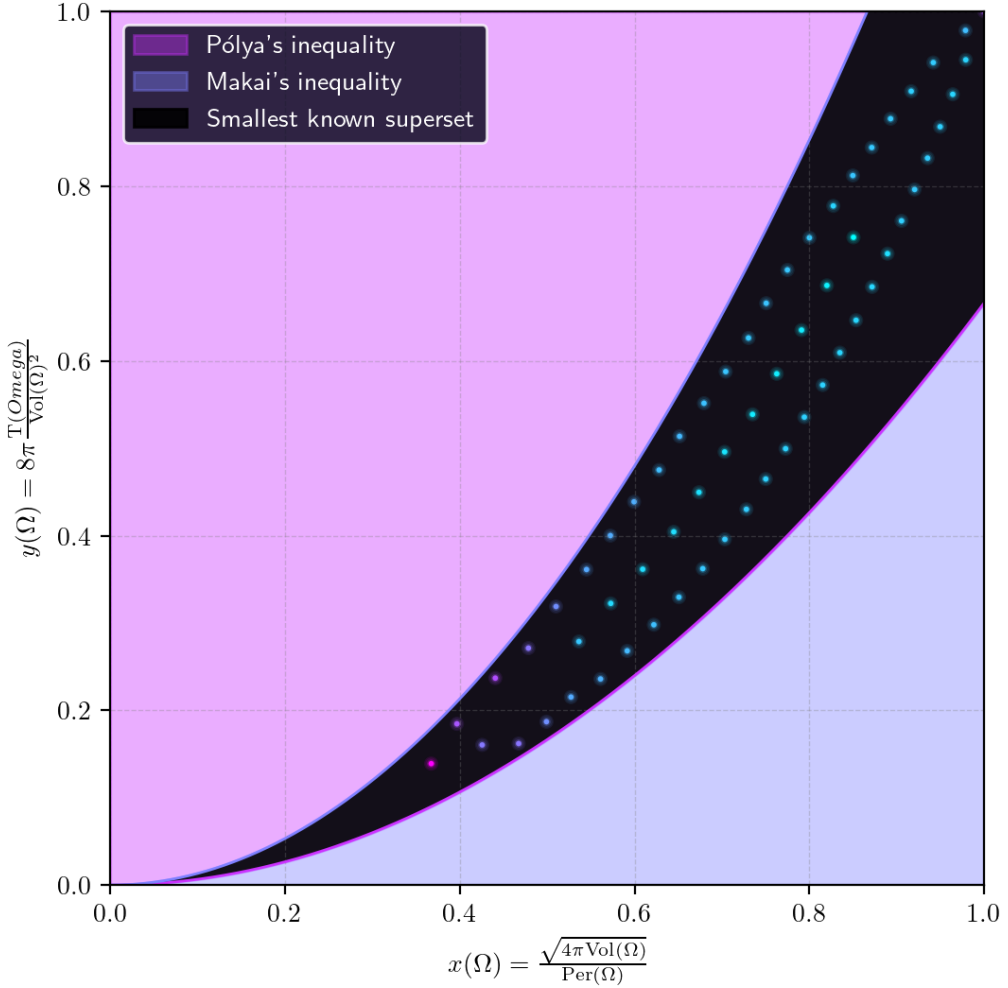


FIGURE 4. Numerical approximation of the diagram \mathcal{D}_{VPT}^2 for $d = 2$ along with the smaller theoretically known superset.

The Weinberger and Bucur–Henrot inequalities translate, respectively, into $x(\Omega) \leq 1$ and $y(\Omega) \leq 1$, which means that

$$\mathcal{D}_{V\mu}^2 := \{(x(\Omega), y(\Omega)) : \Omega \in \mathcal{K}_2\} \subset [0, 1]^2.$$

Note that since we only consider convex sets, we have $y(\Omega) < 1$, the optimal value being unknown. We refer to [4, Section 3] for numerical results on the maximizer of $\text{Vol}(\Omega)\mu_2(\Omega)$ among planar convex sets. Because of the ordering of the eigenvalues, we also have $\text{Vol}(\Omega)\mu_1(\Omega) \leq \text{Vol}(\Omega)\mu_2(\Omega)$. Since $\text{Vol}(B \sqcup B)\mu_2(B \sqcup B) = 2\text{Vol}(B)\mu_1(B)$, this leads to the inequality

$$x(\Omega) \leq 2y(\Omega).$$

Meanwhile, Szegő [54] showed that for planar and simply connected domains,

$$\frac{1}{\text{Vol}(\Omega)\mu_1(\Omega)} + \frac{1}{\text{Vol}(\Omega)\mu_2(\Omega)} \geq \frac{1}{\text{Vol}(B)\mu_1(B)} + \frac{1}{\text{Vol}(B)\mu_2(B)},$$

which translates, in terms of x and y , to

$$y(\Omega) \leq \frac{x(\Omega)}{4x(\Omega) - 2}.$$

Remark 5.2. In a recent paper [34], K. Funano proved that for every convex body in \mathbb{R}^d the following estimates relating μ_k and μ_{k+1}

$$\mu_k(\Omega) \leq Cd^7\mu_{k+1}(\Omega),$$

where C is a universal constant independent of k and d . In the same vein, he proved for planar convex bodies the following result

$$\mu_k(\Omega) \leq C' \left(\frac{k}{\ell}\right)^2 \mu_\ell(\Omega),$$

where $k \geq \ell$ and C' is a universal constant. When taking $k = 2$ and $\ell = 1$, this result supports the conjecture $\mu_2(\Omega) \leq 4\mu_1(\Omega)$ stated in [5] and numerically observed in [4] and in the present work.

In fig. 5, we present the obtained diagram for the class of planar convex sets. The shapes can be visualized here.

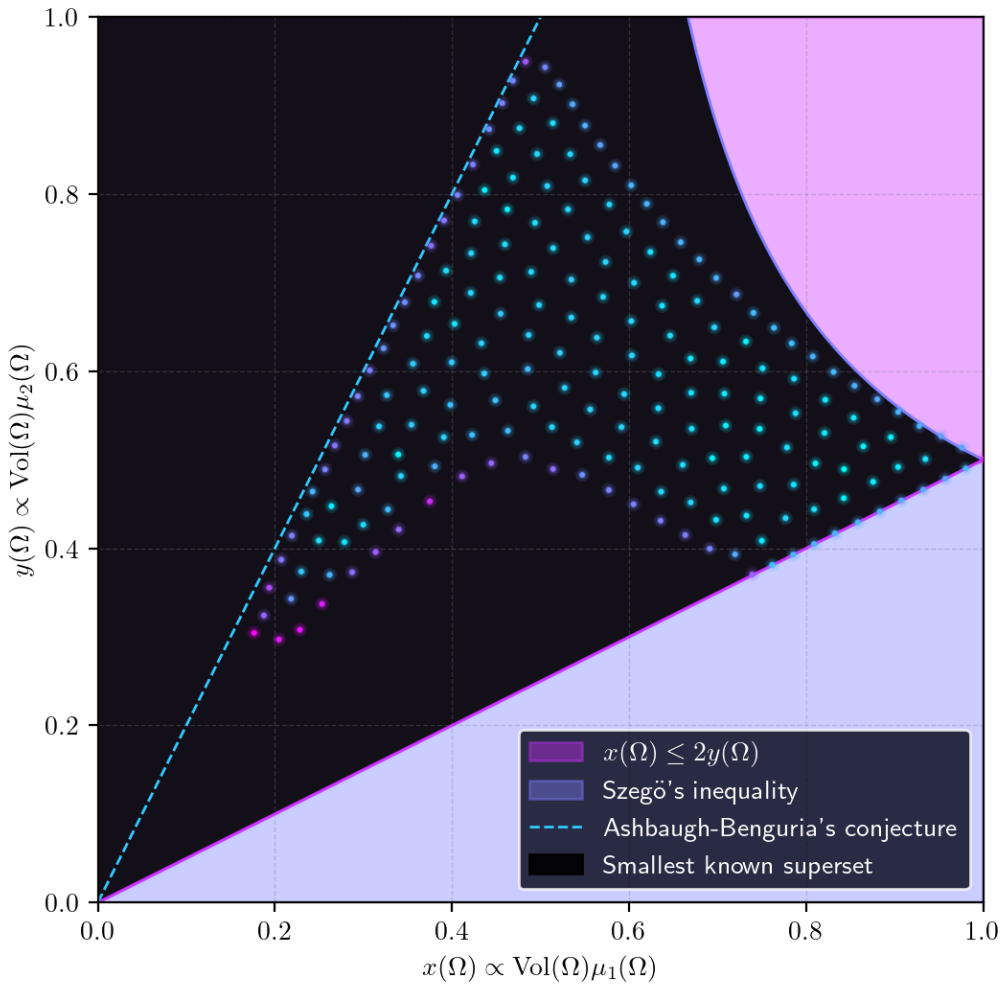


FIGURE 5. Numerical approximation of the diagram $\mathcal{D}_{V\mu}^2$ for $d = 2$ along with the theoretically known smaller superset.

In contrast to the other diagrams, we are not able to recover with high precision the extremal shapes corresponding to the upper part of the boundary of the diagram. In particular, the shapes of the top left part of the boundary appear to be rounded rectangles, although actual rectangles yield a better value (which agrees with the Ashbaugh-Benguria's conjecture). This is due to the fact that because of the approach that we chose, PyTorch needs to differentiate through the whole assembly and the computation of the eigenvalues of eq. (8), which requires a large amount of memory and limits the

quadrature precision. A natural direction for future research is to enhance the memory efficiency of the proposed approach.

5.4. The diagram Vol, Per, E. In this section, we show that our approach can be easily adapted to problems involving higher-order boundary terms, such as the curvature of the boundary. Here, we consider the Willmore energy (also called *elasticae* for the 1 dimensional boundary of planar sets) defined as

$$E(\Omega) := \int_{\partial\Omega} H_{\Omega}^2 d\sigma,$$

where Ω is a C^2 convex body of \mathbb{R}^d and H_{Ω} is the mean curvature of $\partial\Omega$. We note that the functional E is $(d-3)$ -homogeneous and we denote by $\tilde{\mathcal{K}}_d$ the class of C^2 convex bodies of \mathbb{R}^d .

5.4.1. The diagram Vol, Per, E for planar convex sets. In the planar case $d=2$, the functional E is (-1) -homogeneous. We then consider the following scale invariant quantities

$$x(\Omega) := \frac{4\pi \text{Vol}(\Omega)}{\text{Per}(\Omega)^2} \quad \text{and} \quad y(\Omega) := \frac{2\pi^2}{\text{Per}(\Omega)E(\Omega)},$$

and the diagram $\mathcal{D}_{VPE}^2 := \{(x(\Omega), y(\Omega)) : \Omega \in \tilde{\mathcal{K}}_2\}$, which was studied in [9], where qualitative results concerning the diagram and the extremal shapes are established.

The isoperimetric inequality ensures that $x(\Omega) \leq 1$. On the other hand, since

$$2\pi = \int_{\partial\Omega} H_{\Omega} \leq \left(\int_{\partial\Omega} H_{\Omega}^2 \right)^{\frac{1}{2}} \left(\int_{\partial\Omega} 1 \right)^{\frac{1}{2}} = E(\Omega)^{\frac{1}{2}} \text{Per}(\Omega)^{\frac{1}{2}},$$

we have $y(\Omega) \leq 1$. At last, an important inequality, due to Gage [35], states that

$$\frac{E(\Omega)\text{Vol}(\Omega)}{\text{Per}(\Omega)} \geq \frac{\pi}{2},$$

which translates, in our case, to the inequality $y(\Omega) \leq x(\Omega)$.

The resulting diagram is displayed in fig. 6. A visualization of the sets comprising the diagram can be found here.

The lower part of the boundary of the diagram $\{(x, 0) : x \in [0, 1]\}$ is approached by rounded polygons i.e., sets of the form $P_{\varepsilon} = P \oplus B_{\varepsilon}(x)$, where \oplus stands for the Minkowski sum P is a convex polygon and $B_{\varepsilon}(x)$ is a ball of center x and radius ε . Indeed, for any $x^* \in (0, 1)$, there exists a polygon P such that $x(P) = x^*$. Then, one can show that $x(P_{\varepsilon}) \xrightarrow{\varepsilon \rightarrow 0} x^*$ while $E(P_{\varepsilon})$ scales as ε^{-1} .

For the right part of the boundary i.e., $\{(0, y) : y \in [0, 1]\}$, one can approach any point $(0, y^*) \in [0, 1]^2$ by taking sets obtained via Minkowski sums of regular polygons and the unit ball. More precisely, for $N \geq 3$, and $t \in (0, 1]$, we take $R_N^t := (1-t)R_N \oplus tB$, where R_N is the regular polygon of N sides and B is a ball. Finally, it is straightforward that the continuous paths $\Gamma_N := \{x(R_N^t), y(R_N^t) : t \in (0, 1]\} \subset \mathcal{D}_{VPE}^2$ converge to the segment $\{(0, y) : y \in [0, 1]\}$ when N tends to infinity.

5.4.2. The diagram Vol, Per, E for convex sets of dimension three. In dimension three, the Willmore energy is already a scale-invariant functional. Hence, we take

$$x(\Omega) = \frac{36\pi \text{Vol}(\Omega)^2}{\text{Per}(\Omega)^3} \quad \text{and} \quad y(\Omega) = \frac{4\pi}{E(\Omega)},$$

and consider the diagram

$$\mathcal{D}_{VPE}^3 := \{(x(\Omega), y(\Omega)) : \Omega \in \tilde{\mathcal{K}}_3\} \subset [0, 1]^2,$$

where, the normalization in y is motivated by Willmore's inequality

$$E(\Omega) \geq 4\pi,$$

see for instance [1] and the references therein.

The resulting diagram is displayed in fig. 7. A visualization of the sets comprising the diagram can be found here.

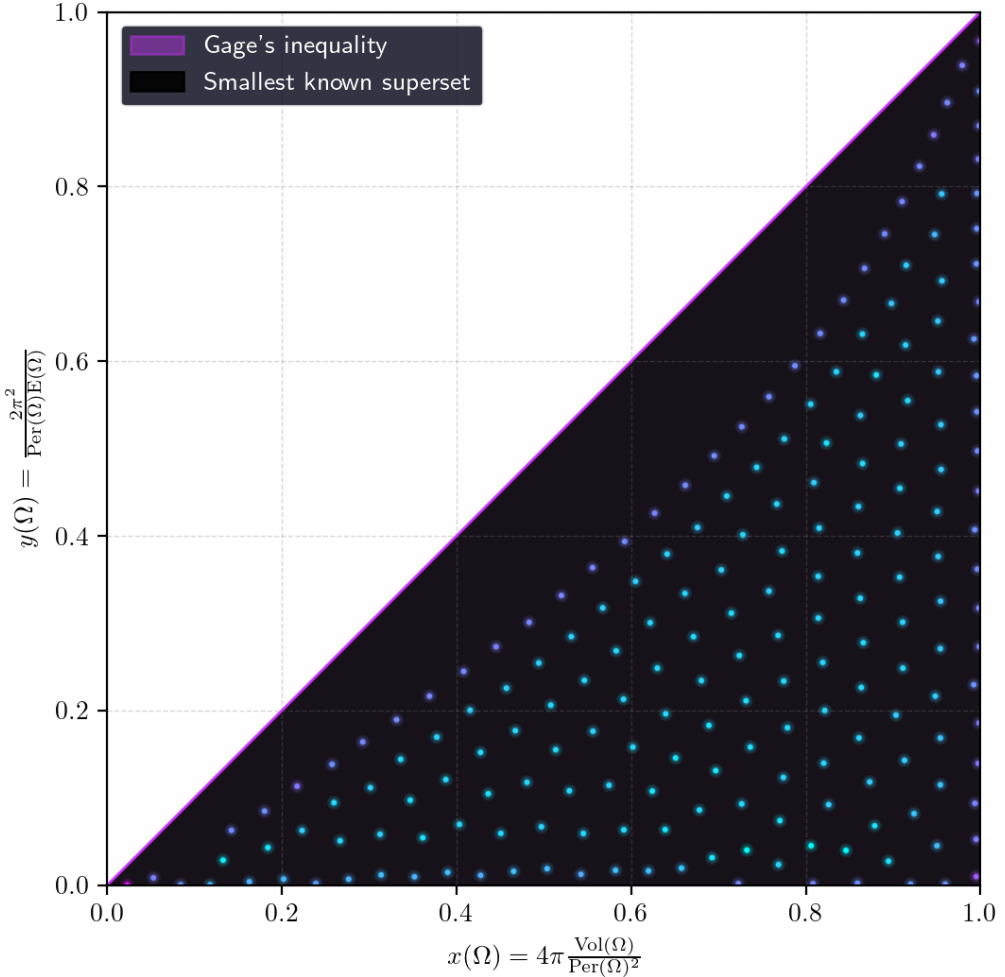


FIGURE 6. Numerical approximation of the diagram \mathcal{D}_{VPE}^2 for $d = 2$ along with the theoretically known smaller superset.

5.5. Limitations of the method. While we have seen through the previous examples that this method is both flexible and robust, it comes with some limitations. First, flexibility and ease of use comes with a price in terms of computation and memory efficiency; indeed, relying on automatic differentiation requires PyTorch to store a large computational graph, particularly when high precision necessitates the use of a substantial number of quadrature points. One potential idea for improvement would be to use higher-order quadrature schemes.

Another limitation comes from the representation itself of the shapes. Since we decided to use a representation *via* gauge functions, some natural geometric quantities associated with convex sets (like the minimal width or the diameter) are harder to compute than when using support functions. However, we note that our proposed parametrization can also be used to parametrize support functions, as every sublinear function p is the support function of the convex set $K = \{y \in \mathbb{R}^d : x \cdot y \leq p(x) \text{ for all } x \in \mathbb{R}^d\}$. However, the computation of quantities relying on change of variables (like the Neumann spectrum) might become more challenging.

5.6. Code availability. For reproducibility purposes, the code used to generate this figures is made fully accessible here: <https://github.com/EloiMartinet/ConvexShapeOpt>. The codes for the generations of the diagrams, listed in the `scripts/` folder, can all run in less than 24 hours on a Nvidia h100 GPU. However, most of them (namely, the purely geometrical ones in two dimensions) needs much less and can also run on CPU in a few hours.

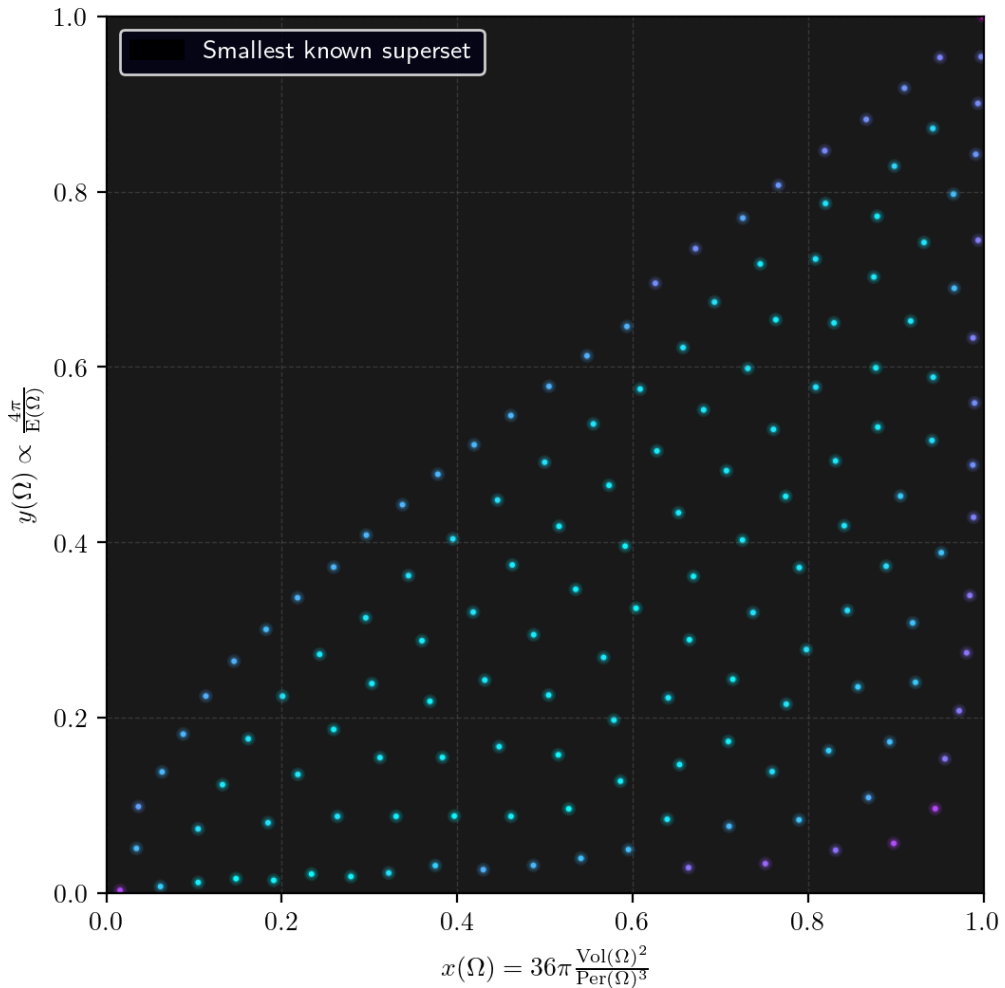


FIGURE 7. Numerical approximation of the diagram \mathcal{D}_{VPE}^3 for $d = 3$.

6. COMPARISON WITH RANDOM SAMPLING

Generating random convex polygons (or, more generally, random convex sets) is a problem of intrinsic interest. In the present work, we employ an algorithm described here, which builds upon the work of P. Valtr [55], where the author computes the probability that a set of n points, independently and uniformly distributed in a given square, is in convex position. As noted in Section 4 of that work, the proof also leads to a fast and "uniform" procedure for generating random convex sets within a prescribed square.

In fig. 8, we compare our results with those obtained via the (naive) Monte Carlo-type method, which consists of generating random convex polygons, computing the associated functionals, and thereby producing a rudimentary approximation of the Blaschke–Santaló diagrams. As can be seen on the figure, the Monte-Carlo method fails to capture certain parts of the diagrams.

7. CONCLUSION AND PERSPECTIVES

In this work, we have introduced a novel numerical framework for the exploration of Blaschke–Santaló diagrams. By leveraging an original invertible neural network architecture to parametrize

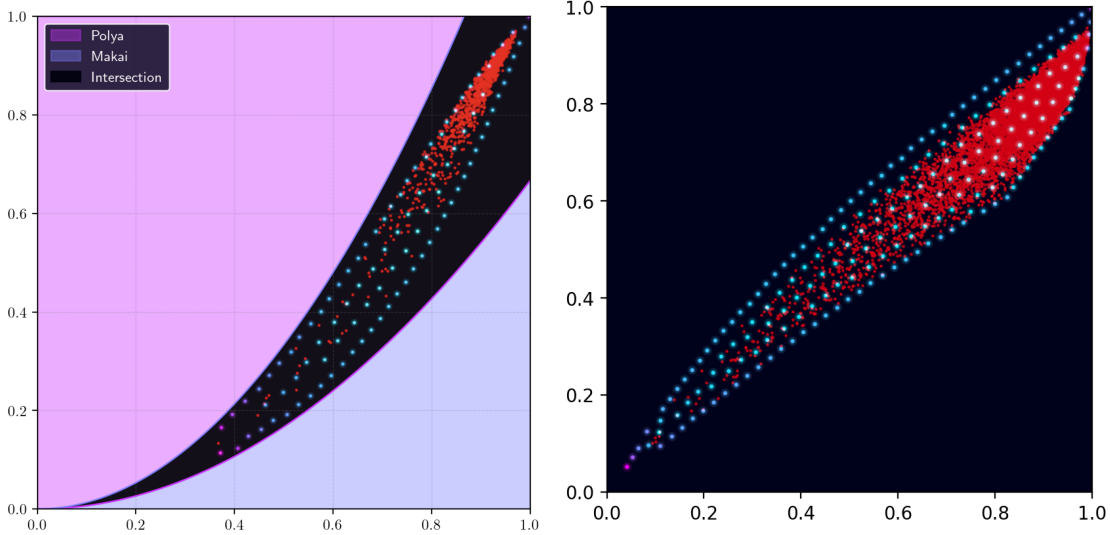


FIGURE 8. Comparison between our results and the ones obtained by random sampling of convex polygons (red dots) for the the diagram $\mathcal{D}_{V\text{PW}}^2$ on the left and the diagram $\mathcal{D}_{V\text{PT}}^2$ on the right.

convex bodies, we developed a fully unconstrained method that avoids handling the convexity constraint explicitly, while it allows to approximate any convex set. We also take advantage of the automatic differentiation capability of PyTorch to handle the complex multi-shape optimization problem that we must solve to uniformly sample the diagrams.

The developed methodology proved highly effective across a diverse range of shape functionals: including purely geometric and PDE-based ones such as the torsional rigidity and the eigenvalues of the Neumann Laplacian. Compared to traditional random sampling of polygons, the proposed method, based on interacting particle systems, yields a substantially more uniform coverage of the diagrams. For the dimensional scalability, it is worth noting that while the computational cost increases in three dimensions due to quadrature requirements, the method remains robust, providing satisfactory descriptions of the diagrams, without any additional implementation difficulties. Lastly, by leveraging automatic differentiation via PyTorch, the framework provides a versatile, easily adaptable system for new functionals, with the complete implementation accessible to the research community.

While the current results focus on the class of convex bodies, the ideas covered in this paper can be extended in several directions:

- **Alternative representations:** One could investigate alternative formulations of sublinear neural networks, for instance by modeling them as a smoothed maximum of the gauge functions of disks rather than of half-spaces. Moreover, combining multiple representations could improve the sampling of Blaschke–Santaló diagrams.
- **General Invertible Architectures:** Extending the parametrization beyond the sublinear functions used here to more general diffeomorphisms of the unit ball. This would allow for the exploration of diagrams for non-convex sets, such as the class of simply connected or star-shaped domains.
- **Further functionals:** Applying the method to more quantities, such as the eigenvalues of higher-order operators or the Cheeger constant, which are notoriously difficult to optimize numerically.
- **Other frameworks:** The underlying idea of sampling the image of a function can be transferred to other research areas, such as periodic homogenization theory, to systematically explore the set of achievable effective material properties induced by different microstructures.

Acknowledgments: Eloi Martinet would like to thank Charles Dapogny and Leon Bungert for fruitful discussions.

This work was finalized during a stay of Ilias Ftouhi at the Isaac Newton Institute for Mathematical Sciences, Cambridge, in February 2026 during the program “Geometric spectral theory and applications”. The author is grateful to the Institute for the very good and stimulating atmosphere. This work was partially supported by EPSRC grant EP/Z000580/1.

The authors acknowledge the use of ChatGPT (OpenAI) to assist in generating preliminary code templates. All generated outputs were thoroughly reviewed, validated, and, where necessary, revised by the authors. ChatGPT was also used for limited language refinement; however, it was not used to generate any substantive scientific content in this manuscript.

REFERENCES

- [1] V. Agostiniani and L. Mazzieri. Monotonicity formulas in potential theory. *Calc. Var. Partial Differential Equations*, 59(1):6, Feb. 2020.
- [2] P. R. S. Antunes and B. Bogosel. Parametric shape optimization using the support function. *Comput. Optim. Appl.*, 82(1):107–138, May 2022.
- [3] P. R. S. Antunes and P. Freitas. New bounds for the principal Dirichlet eigenvalue of planar regions. *Experimental Mathematics*, 15(3):333–342, March 2006.
- [4] P. R. S. Antunes and A. Henrot. On the range of the first two dirichlet and neumann eigenvalues of the laplacian. *Proceedings of the Royal Society A: Mathematical, Physical and Engineering Sciences*, 467(2130):1577–1603, 12 2010.
- [5] M. S. Ashbaugh and R. D. Benguria. Universal bounds for the low eigenvalues of Neumann Laplacians in n dimensions. *SIAM J. Math. Anal.*, 467(3):557–570, 1993.
- [6] S. Bartels and G. Wachsmuth. Numerical Approximation of Optimal Convex Shapes. *SIAM J. Sci. Comput.*, Apr. 2020.
- [7] T. Bayen and D. Henrion. Semidefinite programming for optimizing convex bodies under width constraints. *Optim. Methods Softw.*, Dec. 2012.
- [8] A. Bélières Frendo, E. Franck, V. Michel-Dansac, and Y. Privat. Volume-preserving geometric shape optimization of the Dirichlet energy using variational neural networks. *Neural Networks*, 184:106957, Apr. 2025.
- [9] C. Bianchini, A. Henrot, and T. Takahashi. Elastic energy of a convex body. *Mathematische Nachrichten*, 289(5):546–574, 2016.
- [10] W. Blaschke. Eine frage über konvexe Körper. *Jahresber. Deutsch. Math. Ver.*, 25:121–125, 1916.
- [11] B. Bogosel. The method of fundamental solutions applied to boundary eigenvalue problems. *J. Comput. Appl. Math.*, 306:265–285, Nov. 2016.
- [12] B. Bogosel. Numerical Shape Optimization Among Convex Sets. *Appl. Math. Optim.*, 87(1):1, Feb. 2023.
- [13] B. Bogosel, G. Buttazzo, and E. Oudet. On the numerical approximation of Blaschke-Santaló diagrams using centroidal Voronoi tessellations. *ESAIM, Math. Model. Numer. Anal.*, 58(1):393–420, 2024.
- [14] B. Bogosel, A. Henrot, and M. Michetti. Optimization of Neumann Eigenvalues Under Convexity and Geometric Constraints. *SIAM J. Math. Anal.*, Nov. 2024.
- [15] K. Böröczky, Jr., M. A. Hernández Cifre, and G. Salinas. Optimizing area and perimeter of convex sets for fixed circumradius and inradius. *Monatsh. Math.*, 138(2):95–110, 2003.
- [16] S. V. Borodachov, D. P. Hardin, and E. B. Saff. *Discrete energy on rectifiable sets*, volume 4. Springer, 2019.
- [17] R. Brandenberg and B. González Merino. A complete 3-dimensional Blaschke-Santaló diagram. *Math. Inequal. Appl.*, 20(2):301–348, 2017.
- [18] R. Brandenberg and B. G. Merino. On (r, d, R) -Blaschke-Santaló diagrams with regular k -gon gauges, 2021.
- [19] R. Brandenberg, B. G. Merino, and M. Runge. A complete system of inequalities for the diameter, in-, and circumradius in the 3-dimensional Euclidean space. Preprint, arXiv:2509.05028 [math.MG] (2025), 2025.
- [20] L. Brasco, C. Nitsch, and A. Pratelli. On the boundary of the attainable set of the Dirichlet spectrum. *Z. Angew. Math. Phys.*, 64(3):591–597, 2013.
- [21] D. Bucur, G. Buttazzo, and I. Figueiredo. On the attainable eigenvalues of the Laplace operator. *SIAM J. Math. Ana.*, 30:527–536, 1999.
- [22] D. Bucur and A. Henrot. Maximization of the second non-trivial Neumann eigenvalue. *Acta Math.*, 222(2):337–361, June 2019.
- [23] G. Buttazzo and A. Pratelli. An application of the continuous Steiner symmetrization to Blaschke-Santaló diagrams. *ESAIM, Control Optim. Calc. Var.*, 27:13, 2021.
- [24] B. De Saint-Venant. Mémoire sur la torsion des prismes. *Mémoires présentés par divers savants à l'Académie des Sciences*, 14:233–560, 1856.
- [25] A. Delyon, A. Henrot, and Y. Privat. The missing (A, D, r) diagram. *Ann. Inst. Fourier (Grenoble)*, 72(5):1941–1992, 2022.

- [26] B. Deng, K. Genova, S. Yazdani, S. Bouaziz, G. Hinton, and A. Tagliasacchi. Cvxnet: Learnable convex decomposition. In *Proceedings of the IEEE/CVF Conference on Computer Vision and Pattern Recognition (CVPR)*, June 2020.
- [27] G. E. Fasshauer. *Meshfree approximation methods with Matlab (With Cd-rom)*, volume 6. World Scientific Publishing Company, 2007.
- [28] I. Ftouhi. On the Cheeger inequality for convex sets. *J. Math. Anal. Appl.*, 504(2):Paper No. 125443, 26, 2021.
- [29] I. Ftouhi. Complete systems of inequalities relating the perimeter, the area and the Cheeger constant of planar domains. *Commun. Contemp. Math.*, 25(10):44, 2023.
- [30] I. Ftouhi. Improved Description of Blaschke–Santaló Diagrams via Numerical Shape Optimization. *Appl. Math. Optim.*, 91(3):55, June 2025.
- [31] I. Ftouhi and A. Henrot. The diagram (λ_1, μ_1) . *Math. Rep., Buchar.*, 24(1-2):159–177, 2022.
- [32] I. Ftouhi and J. Lambolley. Blaschke–Santaló diagram for volume, perimeter, and first Dirichlet eigenvalue. *SIAM J. Math. Anal.*, 53(2):1670–1710, 2021.
- [33] I. Ftouhi, A. L. Masiello, and G. Paoli. Sharp inequalities involving the Cheeger constant of planar convex sets. *ESAIM, Control Optim. Calc. Var.*, 30:40, 2024. Id/No 23.
- [34] K. Funano. Two new universal inequalities for Neumann eigenvalues of the Laplacian on a planar convex domain. *arXiv*, Nov. 2025.
- [35] M. E. Gage. An isoperimetric inequality with applications to curve shortening. *Duke Math. J.*, 50(4):1225–1229, Dec. 1983.
- [36] R. Gastaldello, A. Henrot, and I. Lucardesi. About the Blaschke–Santaló diagram of area, perimeter and moment of inertia. *J. Convex Anal.*, 31(2):563–602, 2024.
- [37] Á. González. Measurement of Areas on a Sphere Using Fibonacci and Latitude–Longitude Lattices. *Math. Geosci.*, 42(1):49–64, Jan. 2010.
- [38] I. Goodfellow, D. Warde-Farley, M. Mirza, A. Courville, and Y. Bengio. Maxout networks. In *Proceedings of the 30th International Conference on Machine Learning*, volume 28 of *Proceedings of Machine Learning Research*, pages 1319–1327, Atlanta, Georgia, USA, 17–19 June 2013.
- [39] A. Henrot and M. Pierre. *Shape variation and optimization*, volume 28 of *EMS Tracts in Mathematics*. European Mathematical Society (EMS), Zürich, 2018. A geometrical analysis.
- [40] J. G. Hoskins and S. Steinerberger. Towards optimal gradient bounds for the torsion function in the plane. *J. Geom. Anal.*, 31(8):7812–7841, 2021.
- [41] T. Lachand-Robert and É. Oudet. Minimizing within Convex Bodies Using a Convex Hull Method. *SIAM J. Optim.*, July 2006.
- [42] I. Lucardesi and D. Zucco. On Blaschke–Santaló diagrams for the torsional rigidity and the first Dirichlet eigenvalue. *Ann. Mat. Pura Appl. (4)*, 201(1):175–201, 2022.
- [43] E. Makai. On the principal frequency of a membrane and the torsional rigidity of a beam. In *Studies in mathematical analysis and related topics*, pages 227–231. Stanford Univ. Press, Stanford, Calif., 1962.
- [44] E. Martinet. Shape optimisation using invertible neural networks, (in preparation).
- [45] E. Martinet and L. Bungert. Meshless Shape Optimization Using Neural Networks and Partial Differential Equations on Graphs. In *Scale Space and Variational Methods in Computer Vision*, pages 285–297. Springer, Cham, Switzerland, May 2025.
- [46] D. Mazzoleni and D. Zucco. Convex combinations of low eigenvalues, Fraenkel asymmetries and attainable sets. *ESAIM, Control Optim. Calc. Var.*, 23(3):869–887, 2017.
- [47] É. Oudet. Numerical minimization of eigenmodes of a membrane with respect to the domain. *ESAIM Control Optim. Calc. Var.*, 10(3):315–330, 2004.
- [48] É. Oudet. Shape Optimization Under Width Constraint. *Discrete Comput. Geom.*, 49(2):411–428, Mar. 2013.
- [49] A. Paszke, S. Gross, F. Massa, A. Lerer, J. Bradbury, G. Chanan, T. Killeen, Z. Lin, N. Gimelshein, L. Antiga, A. Desmaison, A. Köpf, E. Yang, Z. DeVito, M. Raison, A. Tejani, S. Chilamkurthy, B. Steiner, L. Fang, J. Bai, and S. Chintala. PyTorch: An Imperative Style, High-Performance Deep Learning Library. *arXiv*, Dec. 2019.
- [50] G. Pólya. Two more inequalities between physical and geometrical quantities. *J. Indian Math. Soc. (N.S.)*, 24:413–419 (1961), 1960.
- [51] G. Pólya. On the role of the circle in certain variational problems. *Ann. Univ. Sci. Budapest. Rolando Eötvös, Sect. Math.*, 3-4:233–239, 1961.
- [52] G. Pólya and G. Szegő. *Isoperimetric Inequalities in Mathematical Physics. (AM-27)*. Princeton University Press, Princeton, NJ, USA, 1951.
- [53] L. Santaló. Sobre los sistemas completos de desigualdades entre tres elementos de una figura convexa plana. *Math. Notae*, 17:82–104, March 1961.
- [54] G. Szegő. Inequalities for certain eigenvalues of a membrane of given area. *J. Ration. Mech. Anal.*, 3:343–356, 1954.
- [55] P. Valtr. Probability that n random points are in convex position. *Discrete Comput. Geom.*, 13(3-4):637–643, 1995.
- [56] H. F. Weinberger. An isoperimetric inequality for the n -dimensional free membrane problem. *Journal of Rational Mechanics and Analysis*, 5(4):633–636, 1956.

[57] H. Wendland. Meshless galerkin methods using radial basis functions. *Mathematics of Computation*, 68(228):1521–1531, 1999.

(Eloi Martinet) INSTITUTE OF MATHEMATICS, UNIVERSITY OF WÜRZBURG, GERMANY
Email address: `eloi.martinet@uni-wuerzburg.de`

(Ilias Ftouhi) LABORATOIRE MIPA, NÎMES UNIVERSITY, SITE DES CARMES, PLACE GABRIEL PÉRI, 30000 NÎMES, FRANCE
Email address: `ilias.ftouhi@unimes.fr`